Schweizerischer Erdbebendienst
Service Sismologique Suisse
Servizio Sismico Svizzero
Swiss Seismological Service

ETH zürich

Basel - Wirtschaftsgymnasium (SBAW)

SITE CHARACTERIZATION REPORT

Clotaire MICHEL, Manuel HOBIGER, Carlo CAUZZI

Valerio POGGI, Jan BURJANEK, Donat FÄH

Sonneggstrasse 5 CH-8092 Zürich Switzerland; E-mail: clotaire.michel@sed.ethz.ch

Last modified : July 15, 2015

Abstract

Ambient vibration array measurements were performed to characterize the site Basel Wirtschaftsgymnasium, in the St Alban district. The site, where the new station SBAW of the Swiss Strong Motion Network was installed, is located on an alluvial terrace of the Rhine in the city of Basel. The new station was installed in the frame of the Basel Erdbebenvorsorge project. In order to characterize the velocity profile under the station, array measurements with $240\,\mathrm{m}$ aperture were performed. The measurements were successful and allowed deriving a velocity model for this site. Inversions with Love and Rayleigh dispersion curves lead to different velocity profiles, with larger velocity values from 1 to $150\,\mathrm{m}$ depth using Love curve. The Quaternary and Tertiary sediments are stiff from $500\,\mathrm{m/s}$ near the surface up to $1200\,\mathrm{m/s}$ at the base of the Tertiary. The interface with the Mesozoic basement takes place between 600 and $700\,\mathrm{m}$ depth. It is producing the fundamental peak in the ellipticity at $0.50\,\mathrm{Hz}$. $V_{s,30}$ is $524\,\mathrm{m/s}$, which would correspond to ground type B in the Eurocode 8 [CEN, 2004] and SIA261 [SIA, 2014]. The theoretical 1D SH transfer function computed from the inverted profiles shows amplifications up to a factor 3 at some resonance frequencies and matches the observed amplification at the station under earthquake.

Contents

1 Introduction

The station SBAW (Basel - Wirtschaftsgymnasium) is part of the dense array of the Swiss Strong Motion Network (SSMNet) in Basel. SBAW has been installed in the framework of the Basel Erdbebenvorsorge project in 2013 as a new station. This project also includes the site characterization. Passive array measurements have been selected as a standard tool to investigate these sites. An array measurement campaign was carried out on 3rd March 2014 in an area with several school buildings including the Wirtschaftsgymnasium and the Fachmaturitätsschule (Fig. 1), with a centre close to SBAW, in order to characterize the velocity profile under this station. This station is located on an alluvial terrace of the Rhine. This report presents the measurement setup, the results of the H/V analysis and of the array processing of the surface waves (dispersion curves). Then, an inversion of these results into velocity profiles is performed. Standard parameters are derived to evaluate the amplification at this site.

Canton	City	Location	Station code	Site type	Slope
Basel Stadt	Basel	Wirtschaftgymnasium	SBAW	Alluvial terrace	Flat

Table 1: Main characteristics of the study-site.

Figure 1: Picture of the site.

2 Geology

The station is located within the deepest part of the Rhine graben where resonance from Tertiary and Quaternary sediments is expected. Moreover, it is located in the deepest part of the St. Jakob-Tüllingen syncline with deeper Tertiary deposits. The geological map indicates that the site is located on an alluvial terrace of the Rhine. A borehole nearby is showing that the quaternary sediments are approximately $15\,\mathrm{m}$ thick and lay on the Molasse alsacienne (molassic marls and sands of Chattian age, Tertiary). Its thickness is unknown but it lays on the Septarienton formation (formerly known as Meletta layers), a calcareous mudstone of Rupelian age. The Sannoisian marl (Tertiary), formerly assumed as the geophysical bedrock, is expected between 330 and $450\,\mathrm{m}$ depth, based on interpolation. Following the interpretation of the Otterbach-2 VSP measurement, the geophysical basement is supposed to be the Mesozoic basement (limestone). It is expected between 520 and $680\,\mathrm{m}$ depth from cross-sections of the syncline.

3 Experiment description

3.1 Ambient Vibrations

The ground surface is permanently subjected to ambient vibrations due to:

- natural sources (ocean and large-scale atmospheric phenomena) below $1\,\mathrm{Hz}$,
- local meteorological conditions (wind and rain) at frequencies around $1\,\mathrm{Hz}$,
- human activities (industrial machines, traffic…) at frequencies above $1\,\mathrm{Hz}$ [Bonnefoy-Claudet et al., 2006].

The objective of the measurements is to record these ambient vibrations and to use their propagation properties to infer the underground structure. First, the polarization of the recorded waves (H/V ratio) is used to derive the resonance frequencies of the soil column. Second, the arrival time delays at many different stations are used to derive the velocity of surface waves at different frequencies (dispersion). The information (H/V, dispersion curves) is then used to derive the properties of the soil column using an inversion process.

3.2 Equipment

For these measurements 11 Quanterra Q330 dataloggers named NR02 to NR12 and 14 Lennartz 3C 5 s seismometers were available (see Tab. 2). Each datalogger can record on 2 ports A (channels EH1, EH2, EH3 for Z, N, E directions) and B (channels EH4, EH5, EH6 for Z, N, E directions). Time synchronization was ensured by GPS. The sensors were placed on a metal tripod, in a $20\,\mathrm{cm}$ deep hole, when necessary, for better coupling with the ground.

Digitizer	Model	Number	Resolution
	Quanterra Q330	11	24 bits
Sensor type	**Model**	**Number**	**Cut-off frequency**
Velocimeter	Lennartz 3C	14	0.2 Hz

Table 2: Equipment used.

3.3 Geometry of the arrays

Two array configurations were used, for a total of 4 rings of 10, 30, 60 and 120 m radius around a central station. The first configuration includes the 3 inner rings with 14 sensors; the second configuration includes the 2 outer rings (plus 1 sensor of the first ring) with 12 sensors. The minimum inter-station distance and the aperture are therefore 10 and 120 m and 10 and 240 m, respectively. The experimental setup is displayed in Fig. 2. The final usable datasets are detailed in section 4.2.

Figure 2: Geometry of the arrays (top: first configuration, bottom: second configuration).

3.4 Positioning of the stations

The sensor coordinates were measured using a differential GPS device (Leica Viva GS10), including only a rover station and using the Real Time Kinematic technique provided by Swisstopo. It allows an absolute positioning with an accuracy better than 6 cm on the Swissgrid. However, this accuracy was not reached at several points due to trees and buildings. The less ac-

curate points were: BAW202 with $57\,\mathrm{cm}$, BAW101 with $18\,\mathrm{cm}$, BAW102 with $18\,\mathrm{cm}$, BAW304 with $11\,\mathrm{cm}$ and BAW305 with $10\,\mathrm{cm}$.

4 Data quality

4.1 Usable data

The largest time windows were extracted, for which all the sensors of the array were correctly placed and the GPS synchronization was ensured. Recordings are very consistent on the whole frequency band. Some sensors have higher noise levels above $10\,\mathrm{Hz}$ due to local noise sources. Spurious peaks, particularly at $1.13\,\mathrm{Hz}$, are noticed as for many others sites in Basel.

Orientations of the sensors were checked by maximizing the correlation with the central station at low frequencies [Poggi et al., 2012b]. Deviations lower than $10\,^\circ$ were found for all points but BAW205 ($21\,^\circ$) and BAW302 ($21\,^\circ$). Original and rotated datasets are available for the 3C array analysis.

The characteristics of the datasets are detailed in Tab. 3.

4.2 Data processing

The data were first converted to SAC format including in the header the coordinates of the point (CH1903 system), the recording component and a name related to the position. The name is made of 3 letters characterizing the location (BAW here), 1 digit for the ring and 2 more digits for the number in the ring. Recordings were not corrected for the instrumental response.

Dataset	**Starting Date**	**Time**	**Length**	F_s	**Min. inter-distance**	**Aperture**	**# of points**
1	2014/03/03	10:41	$123\,\mathrm{min}$	$200\,\mathrm{Hz}$	$10\,\mathrm{m}$	$120\,\mathrm{m}$	14
2	2014/03/03	13:30	$124\,\mathrm{min}$	$200\,\mathrm{Hz}$	$10\,\mathrm{m}$	$240\,\mathrm{m}$	12

Table 3: Usable datasets.

5 H/V processing

5.1 Processing method and parameters

In order to process the H/V spectral ratios, several codes and methods were used. The classical H/V method was applied using the Geopsy `http://www.geopsy.org` software. In this method, the ratio of the smoothed Fourier Transform of selected time windows are averaged. Tukey windows (cosine taper of 5% width) of $50\,\mathrm{s}$ long overlapping by 50% were selected. Konno and Ohmachi [1998] smoothing procedure was used with a b value of 60. The classical method computed using the method of Fäh et al. [2001] was also performed.

Moreover, the time-frequency analysis method [Fäh et al., 2009] was used to estimate the ellipticity function more accurately using the Matlab code of V. Poggi. In this method, the time-frequency analysis using the Wavelet transform is computed for each component. For each frequency, the maxima over time (10 per minute with at least $0.1\,\mathrm{s}$ between each) in the TFA are determined. The Horizontal to Vertical ratio of amplitudes for each maximum is then computed and statistical properties for each frequency are derived. A Cosine wavelet with parameter 9 is used. The mean of the distribution for each frequency is stored. For the sake of comparison, the time-frequency analysis of Fäh et al. [2001], based on the spectrogram, was also used.

The ellipticity extraction using the Capon analysis [Poggi and Fäh, 2010] (see section on array analysis) was also performed.

Method	Freq. band	Win. length	Anti-trig.	Overlap	Smoothing
Standard H/V Geopsy	$0.2-20\,\mathrm{Hz}$	$50\,\mathrm{s}$	No	50%	K&O 60
Standard H/V D. Fäh	$0.2-20\,\mathrm{Hz}$	$30\,\mathrm{s}$	No	75%	-
H/V TFA D. Fäh	$0.2-20\,\mathrm{Hz}$	Specgram	No	-	-
H/V TFA V. Poggi	$0.2-20\,\mathrm{Hz}$	Cosine wpar=9	No	-	No

Table 4: Methods and parameters used for the H/V processing.

5.2 Results

All points show exactly the same shape in their H/V below $5\,\mathrm{Hz}$ with a complex right flank (Fig. 3). The fundamental peak is found at $0.50\,\mathrm{Hz}$. This corresponds to the resonance of the deep Rhine graben. A second peak is also noticed above $15\,\mathrm{Hz}$ corresponding to the two to four first meters of soil.

Moreover, all the methods to compute H/V ratios are compared at the array centre on Fig. 4, in which the classical methods were divided by $\sqrt{2}$ to correct from the Love wave contribution [Fäh et al., 2001]. The classical and TFA methods match well at high frequencies but large variations are observed at low frequencies. The 3C FK analysis (Capon method) does not have resolution down to the peak but matches perfectly with the H/V analysis at high frequency.

The fundamental peak at the SBAW station is therefore at $0.50\,\mathrm{Hz}$, with a peak amplitude around 3 for the TFA methods. A high frequency peak around $16\,\mathrm{Hz}$ due to the first three meters of soil is expected at the station.

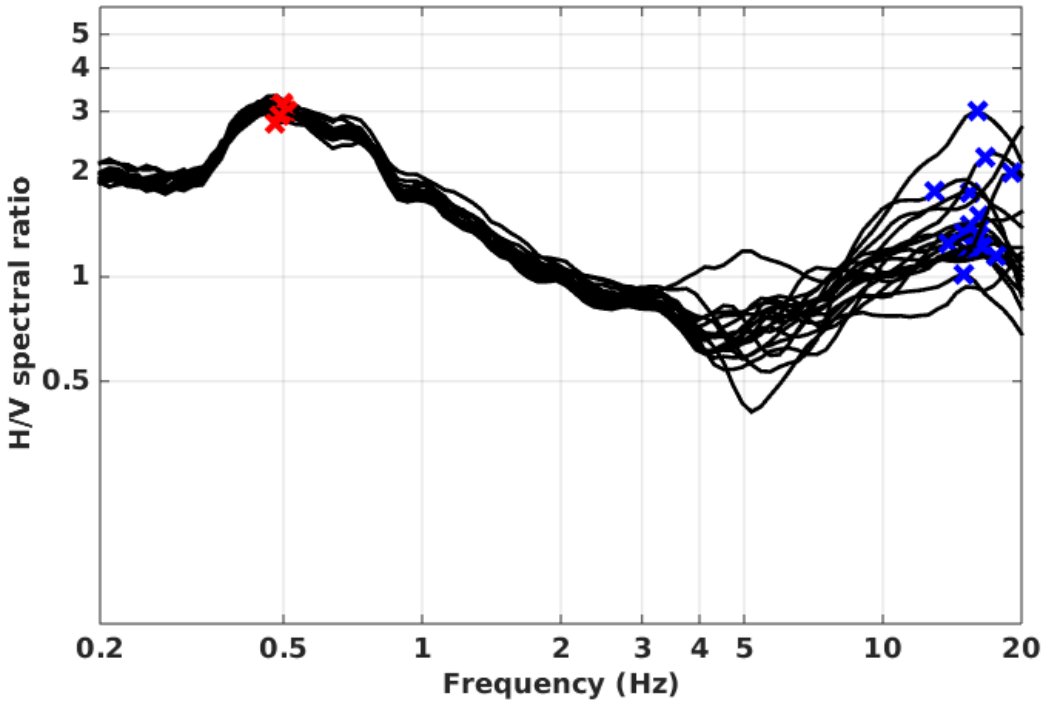

Figure 3: H/V spectral ratios (time-frequency analysis code V. Poggi) of all array points.

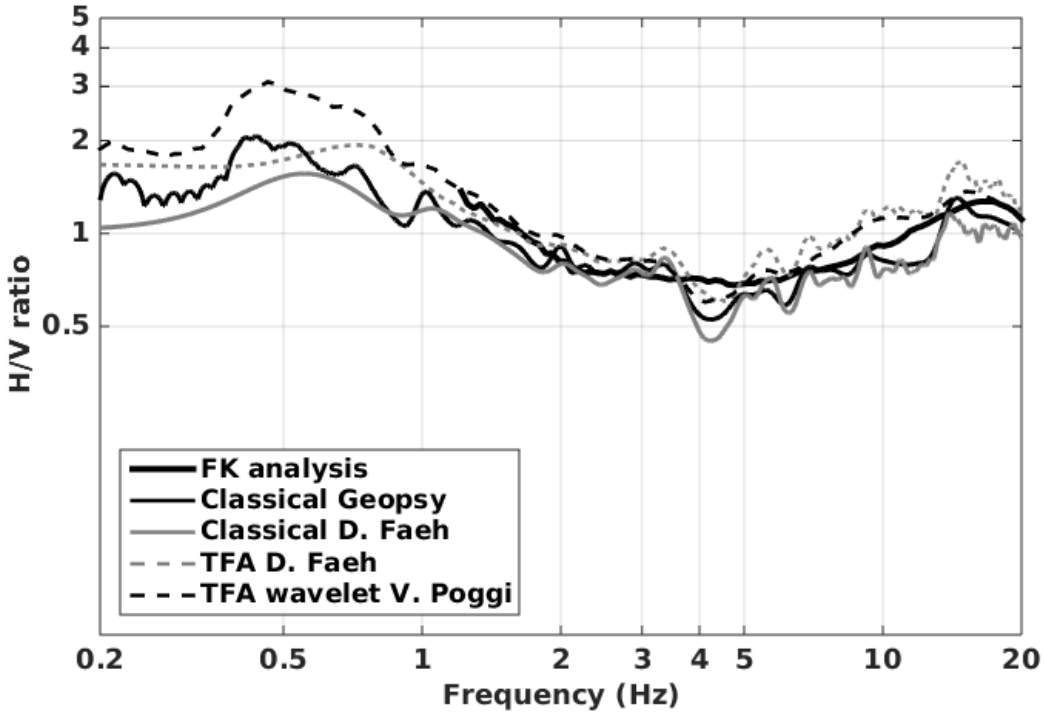

Figure 4: H/V spectral ratios for point BAW000 using the different codes. Classical methods were divided by $\sqrt{2}$.

5.3 Polarization analysis

Considering the shape of the Rhine basin, a 2D resonance could occur. Therefore, polarization analysis on the array data was performed using the method of Burjánek et al. [2010]. The polarization of the spurious peak at $1.13\,\mathrm{Hz}$ is clearly visible. No point (Fig. 5) shows a noticeable polarization at $0.5\,\mathrm{Hz}$ perpendicular to the Rhine graben. 2D resonance is therefore unlikely at this location.

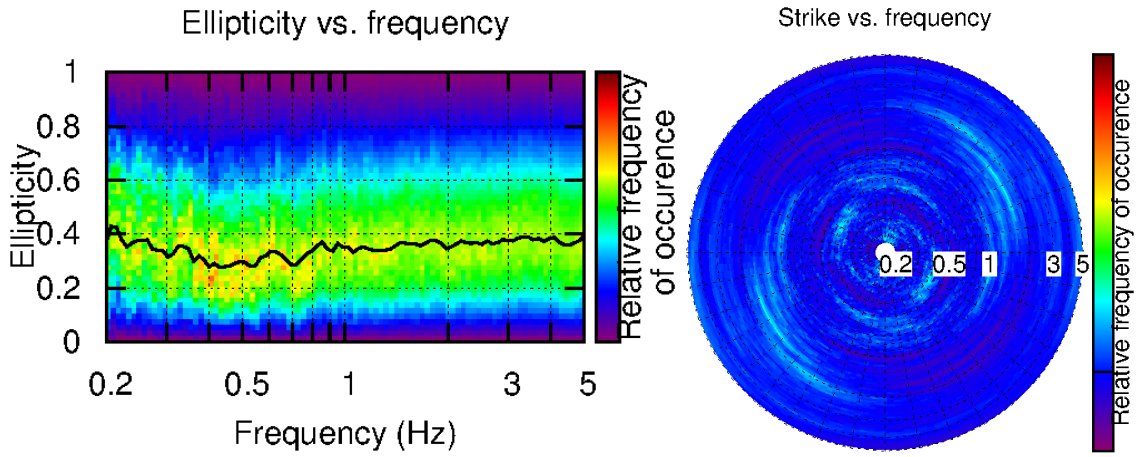

Figure 5: Polarization analysis at point BAW000. Left: Ellipticity (A trough in the ellipticity corresponds to polarized motion). Right: Strike of the polarization.

6 Array processing

6.1 Processing methods and parameters

The vertical components of the arrays were processed using the FK and the High-resolution FK analysis [Capon, 1969] using the Geopsy `http://www.geopsy.org` software. Better results were obtained using large time windows (300T). The results of computations of both datasets were merged to estimate the dispersion curves.

Moreover, a 3C array analysis [Fäh et al., 2008] was also performed using the array_tool_3C software [Poggi and Fäh, 2010]. It allows us to derive Rayleigh and Love modes including the Rayleigh ellipticity. The results of computations of both datasets were merged to estimate the dispersion curves.

Method	Set	Freq. band	Win. length	Anti-trig.	Overlap	Grid step	Grid size	# max.
HRFK 1C	1	$1-25\,\mathrm{Hz}$	$300T$	No	50%	0.001	0.6	5
HRFK 1C	2	$1-25\,\mathrm{Hz}$	$300T$	No	50%	0.001	0.6	5
HRFK 3C	1	$1-25\,\mathrm{Hz}$	Wav. 10	No	50%	300	2000	5
			Tap. 0.2			m/s	m/s	
HRFK 3C	2	$1-25\,\mathrm{Hz}$	Wav. 10	No	50%	300	2000	5
			Tap. 0.2			m/s	m/s	

Table 5: Methods and parameters used for the array processing.

6.2 Obtained dispersion curves

In the 1C FK analysis, the fundamental Rayleigh mode could be picked between $1.5\,\mathrm{Hz}$ and $21\,\mathrm{Hz}$ (Fig. 6), including its standard deviation. The velocities range from $1150\,\mathrm{m/s}$ at $1.5\,\mathrm{Hz}$ on the fundamental mode down to $430\,\mathrm{m/s}$ at $21\,\mathrm{Hz}$. A first higher mode is also visible but has not been not picked.

Using the 3C analysis, fundamental and a higher Rayleigh modes can be picked (Fig. 6). On the radial component, the same modes are seen above $4\,\mathrm{Hz}$. On the transverse component, fundamental Love mode is picked in a similar frequency range as Rayleigh.

All picked curves are presented together on Fig. 7. The fundamental Rayleigh curves are identical for 1C and 3C analysis.

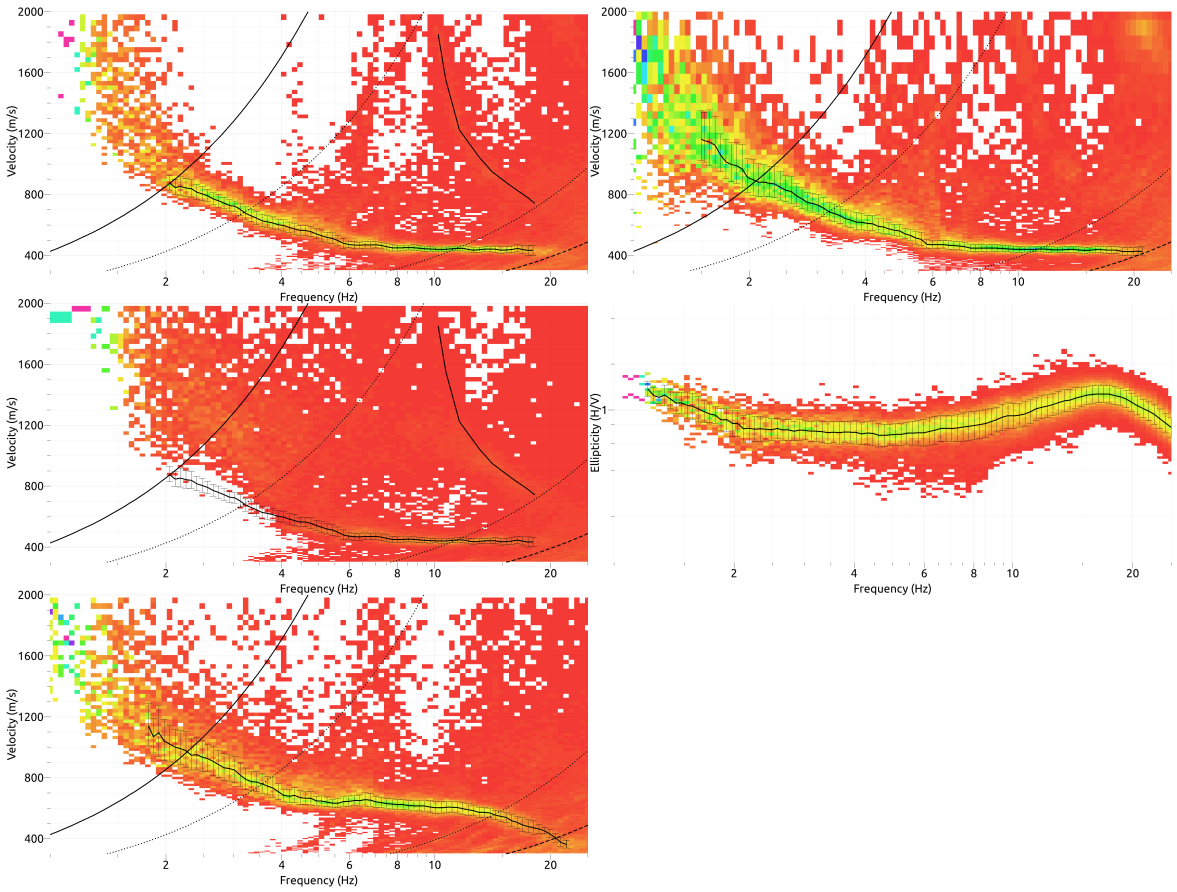

Figure 6: Dispersion curves and ellipticity obtained from the 3C and 1C array analyses (from top to bottom: vertical, radial, transverse components; left: 3C analysis; top right: 1C analysis; centre right: ellipticity).

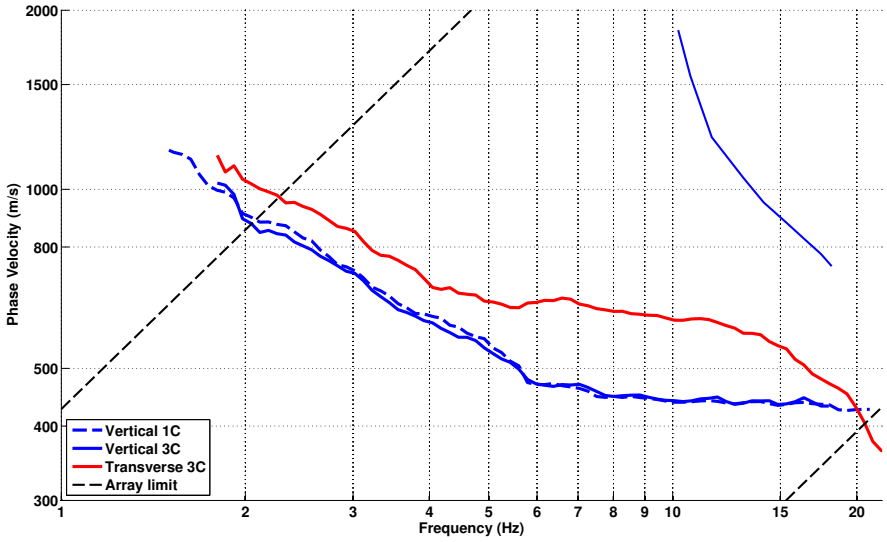

Figure 7: Picked dispersion curves from 1C and 3C FK methods.

7 Inversion and interpretation

7.1 Inversion

For the inversion, the Rayleigh fundamental mode dispersion curve (above $1.9\,\mathrm{Hz}$), the ellipticity curve (TFA Poggi) and the fundamental frequency at $0.50\,\mathrm{Hz}$ were used as simultaneous targets without standard deviation. The higher mode of Rayleigh dispersion found in the FK analysis is most probably the second higher and was not used because of its uncertainty. After many tests, the fundamental Love dispersion curve was discarded for this computation. As in many other locations in Basel, this curve is not compatible with the other targets (too high velocities). A possible explanation could be anisotropy (vertical vs horizontal) in the mudstone of the Septarienton formation but no evidence can be seen on the radial component of such anisotropy. A second inversion was performed using the Love dispersion curve instead of Rayleigh, still using the ellipticity information.

A weight of 0.2 and 0.3 was assigned to the ellipticity curve and 0.1 and 0.2 to the ellipticity peak for these two inversions, respectively. All curves were resampled using 50 points between 0.3 and $22\,\mathrm{Hz}$ in log scale.

The inversion was performed using the Improved Neighborhood Algorithm (NA) [Wathelet, 2008] implemented in the Dinver software. In this algorithm, the tuning parameters are the following: Ns_0 is the number of starting models, randomly distributed in the parameter space, Nr is the the number of best cells considered around these Ns_0 models, Ns is the number of new cells generated in the neighborhood of the Nr cells (Ns/Nr per cell) and It_{max} is the number of iteration of this process. The process ends with $Ns_0 + Nr * \frac{Ns}{Nr} * It_{max}$ models. The used parameters are detailed in Tab. 6.

It_{max}	Ns_0	Ns	Nr
500	10000	100	100

Table 6: Tuning parameters of Neighborhood Algorithm.

No velocity inversion is needed to explain the data although it could be expected at some interfaces. The Poisson ratio was inverted in each layer in the range 0.2-0.4, up to 0.47 in the alluvia, within the groundwater table. The density was assumed to be $2000\,\mathrm{kg/m^3}$ in the sediments and $2700\,\mathrm{kg/m^3}$ in the Mesozoic rock. The velocity of the bedrock is assumed to be $2340\,\mathrm{m/s}$ (from the Otterbach 2 VSP measurement). Inversions with free layer depths as well as fixed layer depths were performed. 4 layers are enough to explain most of the targets (dispersion and ellipticity), but more layers are used to smooth the obtained results and better explore the parameter space. For each assumption (Rayleigh or Love dispersion), 5 independent runs of 5 different parametrization schemes (6 and 7 layers over a half space and 13, two times 15 layers with fixed depth with different values) were performed. Examples of retrieved ground profiles for these two strategies are presented in Fig. 8. When comparing to the target curves for the inversion with the Rayleigh curve (Fig. 9), the Rayleigh fundamental mode is well represented. The higher mode is not matching well. As explained above, the fundamental Love mode is not compatible with this velocity profile. The inversion with Love curve (Fig. 10) also leads to a

good fit of the dispersion curve and even the ellipticity is partially reproduced. None of both inversions is better at reproducing the data.

For further elaborations, the best models of these 2 times 25 runs were selected (Fig. 11). The first meter of the profile shows low velocities (about $200\,\mathrm{m/s}$) that increase quickly in the first $5\,\mathrm{m}$. Below, the velocity is around $500\,\mathrm{m/s}$ down to approximately $45\,\mathrm{m}$ using the Rayleigh dispersion, whereas using the Love dispersion curve, it is to $630\,\mathrm{m/s}$ down to $60\,\mathrm{m}$. No contrast between Quaternary and Tertiary sediments can be seen. With the Rayleigh dispersion, a sharp contrast is clearly seen at $45\,\mathrm{m}$ depth with velocity jumping up to about $780\,\mathrm{m/s}$. With Love dispersion, the contrast occurs slightly deeper, at $60\,\mathrm{m}$ depth, with velocities increasing gradually up to $1200\,\mathrm{m/s}$. In previous works, the first $50\,\mathrm{m}$ with low velocities were interpreted as weathered Tertiary rock and can be seen everywhere in Basel with slightly varying depths. The velocities from the inversion with Rayleigh and Love curves meet at $150\,\mathrm{m}$ depth with a velocity reaching $1200\,\mathrm{m/s}$ at $400\,\mathrm{m}$ depth and remain relatively constant in the Tertiary layers, down to the bedrock. Finally, the bedrock is found between 600 and $700\,\mathrm{m}$ depth, as expected.

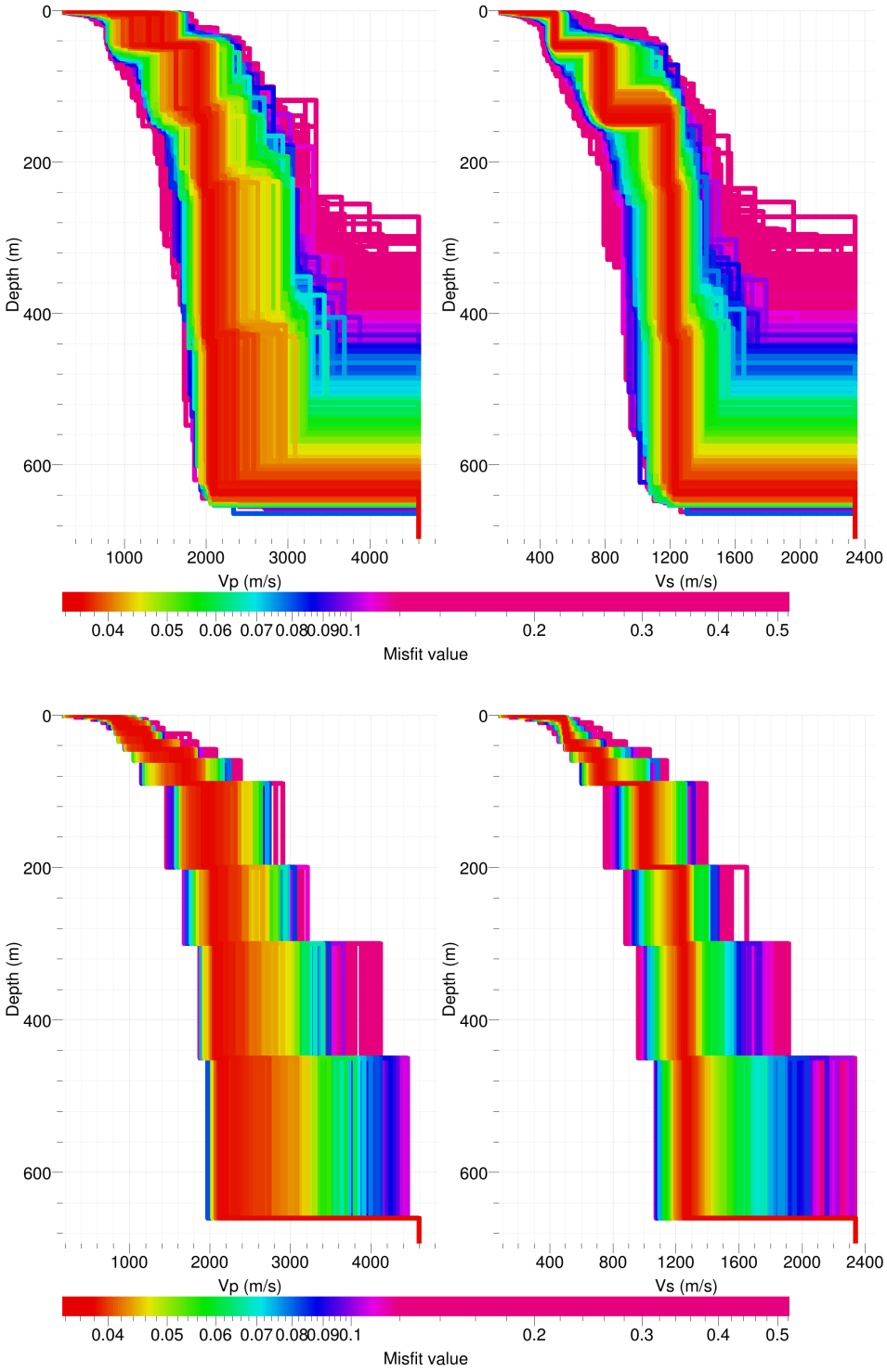

Figure 8: Inverted ground profiles in terms of V_p and V_s; top: free layer depth strategy; bottom: fixed layer depth strategy.

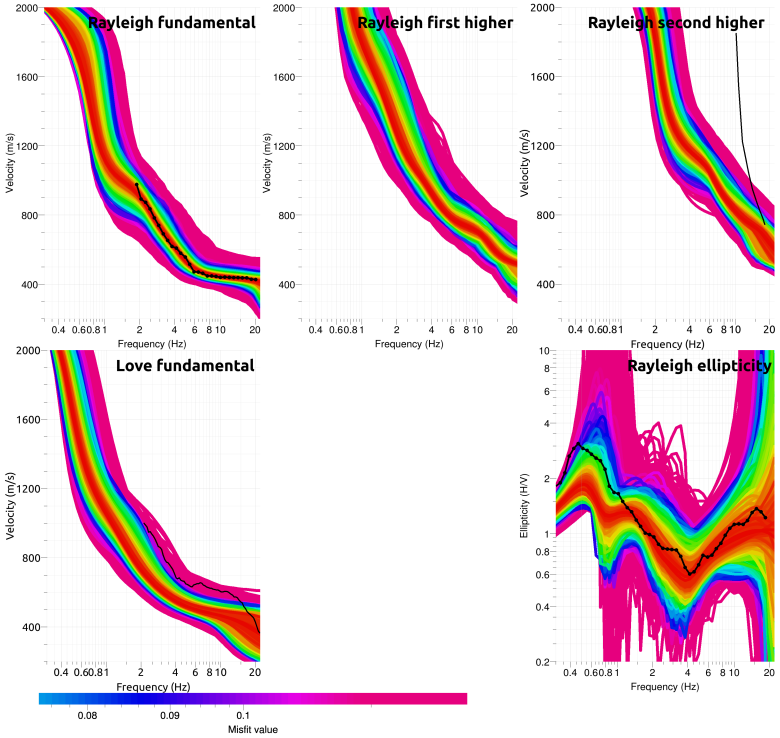

Figure 9: Inversion with Rayleigh curves: comparison between inverted models and measured Rayleigh and Love modes and corresponding ellipticity. Thin black lines were not used in the inversion.

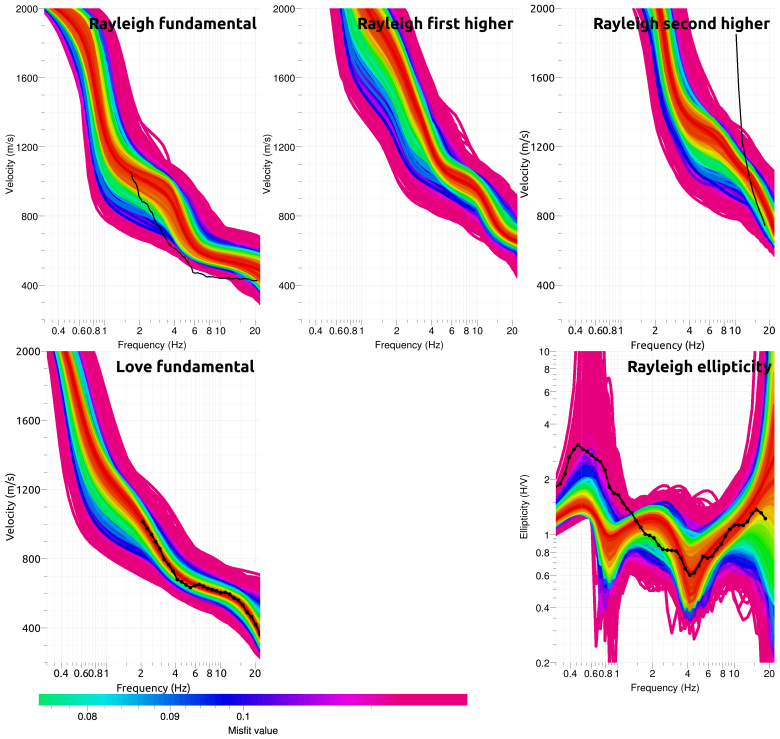

Figure 10: Inversion with Love curves: comparison between inverted models and measured Rayleigh and Love modes and corresponding ellipticity. Thin black lines were not used in the inversion.

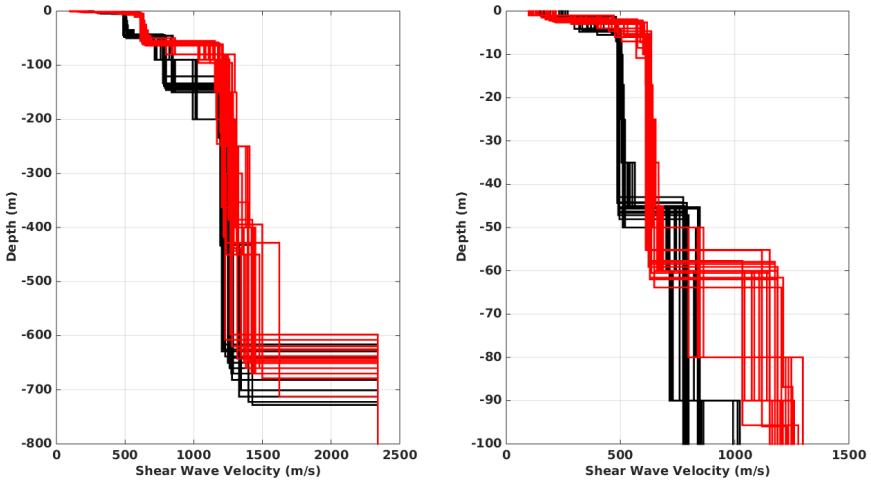

Figure 11: V_s ground profiles for the selected 50 best models. Models from the inversion with Rayleigh (black) and Love (red) curves.

7.2 Travel time average velocities and ground type

The distribution of the travel time average velocities at different depths was computed from the selected models. The uncertainty, computed as the standard deviation of the distribution of travel time average velocities for the considered models, is also provided, but its meaning is doubtful. $V_{s,30}$ is found to be $524\,\mathrm{m/s}$, which corresponds to class B in the Eurocode 8 [CEN, 2004] and the SIA261 [SIA, 2014].

	Mean (m/s)	**Uncertainty (m/s)**
$V_{s,5}$	365	53
$V_{s,10}$	433	48
$V_{s,20}$	496	63
$V_{s,30}$	524	70
$V_{s,40}$	541	75
$V_{s,50}$	557	72
$V_{s,100}$	679	76
$V_{s,150}$	759	85
$V_{s,200}$	827	73

Table 7: Travel time averages at different depths from the inverted models. Uncertainty is given as one standard deviation from the selected profiles.

7.3 SH transfer function and quarter-wavelength velocity

The quarter-wavelength velocity approach [Joyner et al., 1981] provides, for a given frequency, the average velocity at a depth corresponding to 1/4 of the wavelength of interest. It is useful to identify the frequency limits of the experimental data (minimum frequency in dispersion curves at $1.9\,\mathrm{Hz}$ and in the ellipticity at $0.5\,\mathrm{Hz}$ here). The results using this proxy show that the dispersion curves constrain the profiles down to $90\,\mathrm{m}$ and the ellipticity down to $500\,\mathrm{m}$ (Fig. 12). Moreover, the quarter wavelength impedance-contrast introduced by Poggi et al. [2012a] is also displayed in the figure. It corresponds to the ratio between two quarter-wavelength average velocities, respectively from the top and the bottom part of the velocity profile, at a given frequency [Poggi et al., 2012a]. It shows a trough (inverse shows a peak) at the resonance frequency.

Moreover, the theoretical SH-wave transfer function for vertical propagation [Roesset, 1970] is computed from the inverted profiles. It is corrected with respect to the Swiss Reference Rock model [Poggi et al., 2011] following Edwards et al. [2013]. In this case, the models are predicting an amplification up to a factor of 3 at several resonance peaks. The comparison with the Empirical Spectral Modelling (ESM) amplification obtained from earthquake recordings [Edwards et al., 2013] shows a fair agreement.

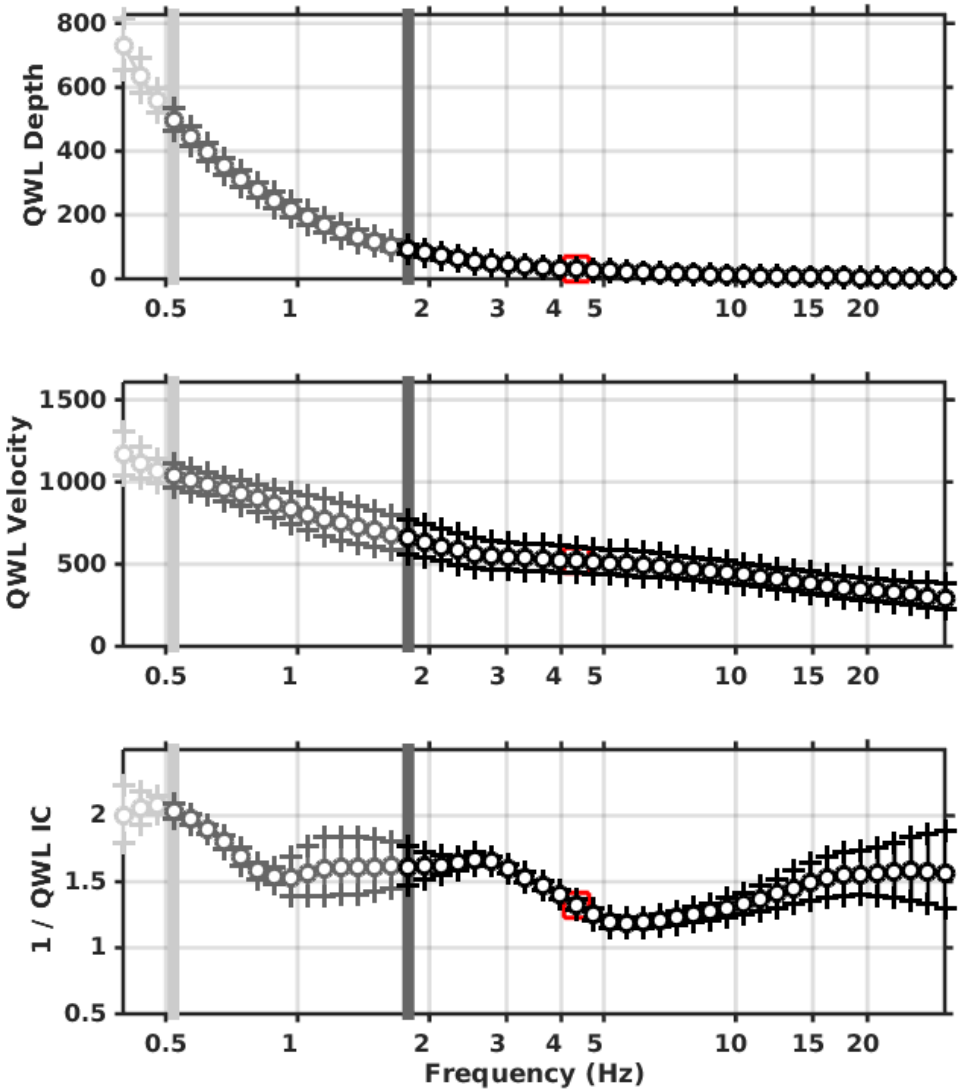

Figure 12: Quarter wavelength velocity representation of the velocity profile (top: depth, centre: velocity, bottom: inverse of the impedance contrast). Black curve is constrained by the dispersion curves, light grey is not constrained by the data. Red square is corresponding to $V_{s,30}$.

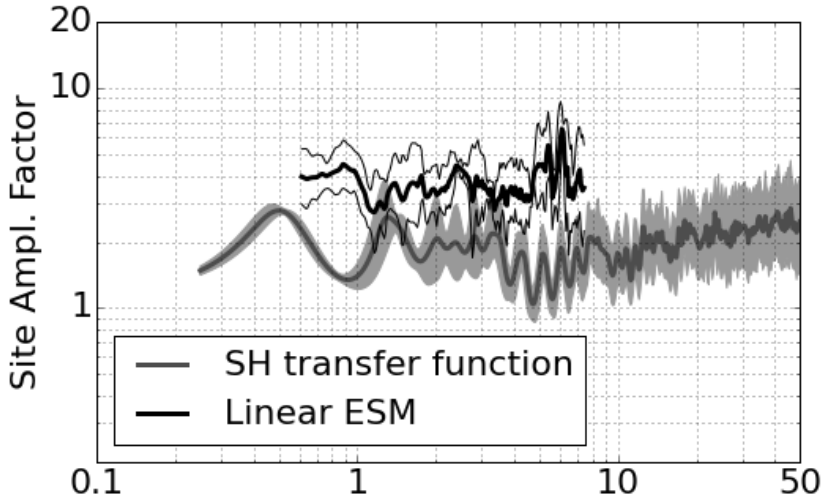

Figure 13: Theoretical SH transfer function (grey line) compared to the empirical spectral amplification [Edwards et al., 2013] (black line) with its standard deviation. Both are referenced at the Swiss Reference Rock Model [Poggi et al., 2011].

8 Conclusions

The array measurements presented in this study were successful in deriving a velocity model for the site Basel Wirtschaftsgymnasium (SBAW station). Inversion with Love and Rayleigh dispersion curves lead to different velocity profiles. Apart from the first meters, we found a first layer of approximately $45\,\mathrm{m}$ with velocities of about $500\,\mathrm{m/s}$ using Rayleigh curves. Using Love curves, the velocity is $630\,\mathrm{m/s}$ down to $60\,\mathrm{m}$ depth. Profiles representative of the Rayleigh and Love dispersion curves deviate until about $150\,\mathrm{m}$ depth. Love dispersion curve provides higher velocities in this depth range, corresponding to the upper part of the Septarienton formation (Tertiary mudstone). It could be due to transverse isotropy (TIV). This kind of anisotropy is associated with layering in shales and is found where gravity is the dominant factor as it is the case for the Septarienton formation. The velocity reaches $1200\,\mathrm{m/s}$ at $150\,\mathrm{m}$ depth until the base of the Tertiary. The interface with the Mesozoic basement takes place between 600 and $700\,\mathrm{m}$ depth. It is producing the fundamental peak in the ellipticity at $0.5\,\mathrm{Hz}$.
$V_{s,30}$ is $524\,\mathrm{m/s}$, which would correspond to ground type B in the Eurocode 8 [CEN, 2004] and SIA261 [SIA, 2014] but is uncertain due to the two families of profiles used for this computation. The theoretical 1D SH transfer function computed from the inverted profiles shows amplifications up to a factor 3 at some resonance frequencies and matches the observed amplification at the station under earthquake.

Acknowledgements

The authors thank Ulrich Aerne for his help during these measurements.

References

Sylvette Bonnefoy-Claudet, Fabrice Cotton, and Pierre,ÄêYves Bard. The nature of noise wavefield and its applications for site effects studies. *Earth-Science Reviews*, 79(3-4): 205–227, December 2006. ISSN 00128252. doi: 10.1016/j.earscirev.2006.07.004. URL http://linkinghub.elsevier.com/retrieve/pii/S0012825206001012.

Jan Burjánek, Gabriela Gassner-Stamm, Valerio Poggi, Jeffrey R. Moore, and Donat Fäh. Ambient vibration analysis of an unstable mountain slope. *Geophysical Journal International*, 180(2):820–828, February 2010. ISSN 0956540X. doi: 10.1111/j.1365-246X.2009.04451.x. URL http://gji.oxfordjournals.org/cgi/doi/10.1111/j.1365-246X.2009.04451.xhttp://doi.wiley.com/10.1111/j.1365-246X.2009.04451.x.

J. Capon. High-Resolution Frequency-Wavenumber Spectrum Analysis. *Proceedings of the IEEE*, 57(8):1408–1418, 1969. ISSN 0018-9219. doi: 10.1109/PROC.1969.7278. URL http://ieeexplore.ieee.org/lpdocs/epic03/wrapper.htm?arnumber=1449208.

CEN. *Eurocode 8: Design of structures for earthquake resistance - Part 1: General rules, seismic actions and rules for buildings*. European Committee for Standardization, en 1998-1: edition, 2004.

Benjamin Edwards, Clotaire Michel, Valerio Poggi, and Donat Fäh. Determination of Site Amplification from Regional Seismicity : Application to the Swiss National Seismic Networks. *Seismological Research Letters*, 84(4), 2013. doi: 10.1785/0220120176.

Donat Fäh, Fortunat Kind, and Domenico Giardini. A theoretical investigation of average H/V ratios. *Geophysical Journal International*, 145(2):535–549, May 2001. ISSN 0956540X. doi: 10.1046/j.0956-540x.2001.01406.x. URL http://doi.wiley.com/10.1046/j.0956-540x.2001.01406.x.

Donat Fäh, Gabriela Stamm, and Hans-Balder Havenith. Analysis of three-component ambient vibration array measurements. *Geophysical Journal International*, 172(1):199–213, January 2008. ISSN 0956540X. doi: 10.1111/j.1365-246X.2007.03625.x. URL http://doi.wiley.com/10.1111/j.1365-246X.2007.03625.xhttp://gji.oxfordjournals.org/cgi/doi/10.1111/j.1365-246X.2007.03625.x.

Donat Fäh, Marc Wathelet, Miriam Kristekova, Hans-Balder Havenith, Brigitte Endrun, Gabriela Stamm, Valerio Poggi, Jan Burjánek, and Cécile Cornou. Using Ellipticity Information for Site Characterisation. Technical report, NERIES JRA4 Task B2, 2009.

William B. Joyner, Richard E. Warrick, and Thomas E. Fumal. The effect of Quaternary alluvium on strong ground motion in the Coyote Lake, California, earthquake of 1979. *Bulletin of the Seismological Society of America*, 71(4):1333–1349, 1981.

Katsuaki Konno and Tatsuo Ohmachi. Ground-Motion Characteristics Estimated from Spectral Ratio between Horizontal and Vertical Components of Microtremor. *Bulletin of the Seismological Society of America*, 88(1):228–241, 1998.

Valerio Poggi and Donat Fäh. Estimating Rayleigh wave particle motion from three-component array analysis of ambient vibrations. *Geophysical Journal International*, 180(1):251–267, January 2010. ISSN 0956540X. doi: 10.1111/j.1365-246X.2009.04402.x. URL http://doi.wiley.com/10.1111/j.1365-246X.2009.04402.x.

Valerio Poggi, Benjamin Edwards, and Donat Fäh. Derivation of a Reference Shear-Wave Velocity Model from Empirical Site Amplification. *Bulletin of the Seismological Society of America*, 101(1):258–274, January 2011. ISSN 0037-1106. doi: 10.1785/0120100060. URL http://www.bssaonline.org/cgi/doi/10.1785/0120100060.

Valerio Poggi, Benjamin Edwards, and Donat Fäh. Characterizing the Vertical-to-Horizontal Ratio of Ground Motion at Soft-Sediment Sites. *Bulletin of the Seismological Society of America*, 102(6):2741–2756, December 2012a. ISSN 0037-1106. doi: 10.1785/0120120039. URL http://www.bssaonline.org/cgi/doi/10.1785/0120120039.

Valerio Poggi, Donat Fäh, Jan Burjánek, and Domenico Giardini. The use of Rayleigh-wave ellipticity for site-specific hazard assessment and microzonation: application to the city of Lucerne, Switzerland. *Geophysical Journal International*, 188(3):1154–1172, March 2012b. ISSN 0956540X. doi: 10.1111/j.1365-246X.2011.05305.x. URL http://doi.wiley.com/10.1111/j.1365-246X.2011.05305.xhttp://gji.oxfordjournals.org/cgi/doi/10.1111/j.1365-246X.2011.05305.x.

J.M. Roesset. Fundamentals of soil amplification. In R. J. Hansen, editor, *Seismic Design for Nuclear Power Plants*, pages 183–244. M.I.T. Press, Cambridge, Mass., 1970. ISBN 978-0-262-08041-5. URL http://mitpress.mit.edu/catalog/item/default.asp?ttype=2&tid=5998.

SIA. *SIA 261 Einwirkungen auf Tragwerke*. Société suisse des ingénieurs et des architectes, Zurich, Switzerland, 2014.

Marc Wathelet. An improved neighborhood algorithm: Parameter conditions and dynamic scaling. *Geophysical Research Letters*, 35(9):1–5, May 2008. ISSN 0094-8276. doi: 10.1029/2008GL033256. URL http://www.agu.org/pubs/crossref/2008/2008GL033256.shtml.